R. & M. No. 3671

R. & M. No. 3671

MINISTRY OF AVIATION SUPPLY

AERONAUTICAL RESEARCH COUNCIL
REPORTS AND MEMORANDA

Low-Speed Wind-Tunnel Measurements of the Oscillatory Lateral Aerodynamic Derivatives of a BAC 221 Model and Comparison of Results with Similar Concorde and HP 115 Data

By C. O. O'LEARY

Aerodynamics Dept., RAE, Bedford

LONDON: HER MAJESTY'S STATIONERY OFFICE
1971
PRICE 85p NET

Low-Speed Wind-Tunnel Measurements of the Oscillatory Lateral Aerodynamic Derivatives of a BAC 221 Model and Comparison of Results with Similar Concorde and HP 115 Data

By C. O. O'LEARY

Aerodynamics Dept., RAE, Bedford

Reports and Memoranda No. 3671*
May, 1970

Summary.

An oscillatory rig has been used to measure a complete set of low-speed lateral derivatives for the BAC 221 slender ogee-wing research aircraft. Tests covered the angle of attack range 0° to 26° and, at some angles of attack, measurements were also made at sideslip angles of $\pm 5°$.

Comparison of the BAC 221 results with Concorde and HP 115 data shows that derivatives due to rate of roll are similar; n_v and particularly $(n_p + n_{\dot{v}} \sin \alpha)$ increase markedly with angle of attack for the HP 115 although not for the Concorde and BAC 221.

*Replaces RAE Tech. Report No. 70095—A.R.C. 32 314.

LIST OF CONTENTS

1. *Introduction.*

The BAC 221 slender ogee-wing research aircraft is currently being tested at the R.A.E. An adequate amount of data from static wind-tunnel tests is available for comparison with flight measurements but there is also a need for dynamic wind-tunnel measurements of, in particular, lateral aerodynamic derivatives. This report describes low-speed tests made in the 13ft × 9ft tunnel at angles of attack up to 26°. A further series of tests at transonic and supersonic speeds is planned. The technique used for oscillatory measurements at R.A.E. Bedford has been described in earlier reports[1,2] and no major changes were made for these tests.

Oscillatory measurements of the lateral derivatives of the HP 115[2] and Concorde were made in previous tests and the derivatives for the three slender aircraft are compared in the report.

2. *Description of Tests.*

2.1. *Brief Account of Method.*

The method of test was basically as described in Ref. 1 and is briefly summarised here. More recent improvements are described in Ref. 2.

The model was mounted on a special sting or spring unit (Fig. 1) which had a forward spring providing flexibilities in yaw and roll and a rear spring providing flexibility in sideslip. Oscillations were excited by means of an electromagnetic vibration generator and the motion was measured by means of accelerometers in the model. The system had three modes of oscillation which were designated yawing, sideslipping and rolling modes. The rolling mode did not generally include much yaw or sideslip but the yawing oscillation had its axis some distance behind the centre of the forward spring and the sideslipping mode included a considerable amount of yawing motion. The test procedure was to oscillate the model at or near the natural frequency of each mode in turn (since this was the only way of obtaining reasonable amplitudes with the small excitation force available). Eighteen derivatives were obtained by solving the complete equations of motion, using measured values of the accelerations and excitation forces (as vectors) and frequencies, together with determined values of the model inertias. The required aerodynamic derivatives were then obtained as the difference between wind-off and wind-on values of the derivatives; (assuming that the mechanical characteristics of the system were unaffected by the air loads). Since the frequencies were different for the different modes, it was necessary when solving the equations of motion to disregard any frequency dependence of the derivatives. This procedure was considered adequate because, in effect, each derivative was obtained primarily from one of the modes with small correction terms from the others. The frequency parameters quoted were those of the primary modes for each derivative. As well as subtracting wind-off values to allow for the characteristics of the spring unit certain other corrections had to be applied because of the effects of the steady aerodynamic normal force and pitching moment. These are explained in Ref. 2.

2.2. *Model and Test Conditions.*

The main dimensions of the model and details of the test conditions are given in Table 1. A sketch of the 1/12 scale BAC 221 glass fibre model is shown in Fig. 2. Engine air intakes under the wing-root leading edges were omitted. Ailerons represented on the model were fixed at 3° up to correspond with the aircraft in flight condition. The ground rigging position was 2° up but owing to a difference in the coefficient of expansion between the control rods and the airframe, the aileron droop changed at high altitude where most tests were made. The movable elevators were driven by an electric motor mounted in the nose, and for trimming during the tests, the elevators could be actuated, remotely, through a range 16·7° up to 0·6° down. Slightly more down elevator should have been available since it was not possible to trim out at zero angle of attack. To allow sufficient sting clearance the jet exit diameter was slightly more than the scale dimension.

The spring unit is shown in Fig. 1. The forward spring was too stiff in roll for the model used in these low-speed tests and resulted in an excessively high roll frequency parameter. For any future tests on models with a roll inertia similar to that of the BAC 221 it is proposed that a spring unit with reduced

roll stiffness will be available. Strain gauges were fitted to the spring unit to allow measurement of normal force, pitching moment, side force, yawing moment and rolling moment for static tests.

At four angles of attack (α) through the test range dynamic measurements were also made at sideslip angles (β)* of $\pm 5°$ and forces and moments were measured statically at 1° intervals from $\beta = -5°$ to 5°. The model was not retrimmed between the $\beta = 0°$ and $\beta = \pm 5°$ tests.

3. *Results.*

3.1. *Presentation.*

As presented in the report the derivatives relate to body axes with the origin at the CG. Model motion is induced relative to the fixed airstream, i.e. to axes fixed in the wind tunnel coincident with the mean position of the oscillating model, the relevant angular displacement parameters being ϕ about the longitudinal model axis and ψ about an axis normal to this longitudinal axis and in the wind tunnel-pitch plane. The translational displacement, y, is coplanar with ψ and normal to the pitch plane. The three modes of oscillation which are primarily rotational in ϕ and ψ and translational in y are referred to as the roll, yaw and sideslip modes respectively. The components of the associated force and moment vectors are measured in an axis system fixed in the model.

The body axis motion parameters are p, v and r, p and r being the components of the angular velocity relative to the earth around the body x and z axes respectively and v the translational velocity component along the body y axis.

Because of the kinematic constraints imposed on the motion of the model certain of the aerodynamic derivatives usually used in the analysis of aircraft dynamics occur in combination. These can be represented by a set of single derivatives, which can be measured directly (N_ψ, N_ϕ etc., or non-dimensionally, n_ψ, n_ϕ etc.). The relationships between this latter set and the other are given below.

$$n_r - n_{\dot{v}} \cos\alpha = n_\phi = N_\phi/(\tfrac{1}{2}\rho\, VSb^2)$$

$$n_p + n_{\dot{v}} \sin\alpha = n_\phi = N_\psi/(\tfrac{1}{2}\rho\, VSb^2)$$

$$y_r - y_{\dot{v}} \cos\alpha = y_\phi = Y_\phi/(\tfrac{1}{2}\rho\, VSb)$$

$$y_p + y_{\dot{v}} \sin\alpha = y_\psi = Y_\psi/(\tfrac{1}{2}\rho\, VSb)$$

$$l_r - l_{\dot{v}} \cos\alpha = l_\phi = L_\phi/(\tfrac{1}{2}\rho\, VSb^2)$$

$$l_p + l_{\dot{v}} \sin\alpha = l_\psi = L_\psi/(\tfrac{1}{2}\rho\, VSb^2)$$

$$-n_{\dot{v}} \cos\alpha = n_\phi = N_\phi/(\tfrac{1}{2}\rho\, V^2Sb)$$

$$n_v = n_{\dot{y}} = N_{\dot{y}}/(\tfrac{1}{2}\rho VSb)^*$$

$$-y_v \cos\alpha = y_\psi = Y_\psi/(\tfrac{1}{2}\rho\, V^2S)$$

$$y = y_{\dot{y}} = Y_{\dot{y}}/(\tfrac{1}{2}\rho\, VS)\dagger$$

$$-l_v \cos\alpha = l_\psi = L_\psi/(\tfrac{1}{2}\rho\, V^2Sb)$$

$$l_v = l_{\dot{y}} = L_{\dot{y}}/(\tfrac{1}{2}\rho\, VSb)\dagger$$

*For the convenience of the reader, α and β as well as u, v, and w are used in this Report to define the orientation of the body to the flight path. The definitions of the incidence and sideslip angles used herein implicitly assume that α and β are respectively applied in this order, so that, in terms of the translational velocity components (u, v, w), they are uniquely defined by

$$\begin{bmatrix} u \\ v \\ w \end{bmatrix} = \begin{bmatrix} \cos\alpha\cos\beta \\ -\sin\beta\cos\alpha \\ \sin\alpha \end{bmatrix} |V|$$

† These sideslipping mode derivatives are not presented in the results (*see* Section 3.3).

3.2. *Longitudinal Static Measurements.*

Normal force, C_z and elevator angle to trim η_T are plotted against angle of attack, α in Fig. 3. It should be noted that there are no points at $\alpha = 0°$ since the model could not be completely trimmed at this angle of attack owing to a mechanical limitation on positive elevator movement.

3.3. *Lateral Dynamic and Static Measurements.*

3.3.1. *Translational velocity derivatives.* The derivatives, n_v, y_v and l_v plotted in Figs. 4, 5, and 6 were obtained from yawing mode measurements of n_ψ, y_ψ and l_ψ respectively. In principle, n_v, y_v and l_v could also have been obtained from the side-slipping mode, since they are identical to $n_{\dot{y}}$, $y_{\dot{y}}$ and $l_{\dot{y}}$. Unfortunately, model radius of gyration and position on the spring unit were such that it was not possible to obtain results of reasonable accuracy from the sideslipping mode. An excessive amount of yawing was present in this mode and this meant that equations for $N_{\dot{y}}$, $Y_{\dot{y}}$ and $L_{\dot{y}}$ contained large 'correction' terms which degraded these results. There were, however, no systematic errors.

A comparison of the results for $\beta = 0°$, and $\beta = \pm 5°$ shows that, throughout the range of angle of attack, there are only small changes in n_v (Fig. 4) and y_v (Fig. 5), but at $\alpha = 24°$, l_v at $\beta = \pm 5°$ is half* that at $\beta = 0°$ and a smaller reduction is evident at $\alpha = 20°$ (Fig. 6). There is some discrepancy between n_v and y_v for $\beta = 5°$ and $\beta = -5°$. It is likely that much of this variation is caused by model asymmetry. Static tests also yielded values of n_v, y_v and l_v from the slopes of plots of yawing moment, side force and rolling moment against sideslip angle shown in Figs. 7, 8 and 9. The slopes were measured over a range of $\pm 1°$ sideslip to match the amplitude of the dynamic tests. The static and dynamic measurements for $\beta = 0°$ agree quite well but results for $\beta = +5°$ cannot properly be compared since static tests were not extended beyond $\pm 5°$ sideslip. However, slopes derived from the dynamic results are shown in Figs. 7, 8 and 9 and in most cases there is fair agreement with the appropriate static results. The incidence at which n_v changes sign, 22° for $\beta = 0°$, coincides with vortex bursting observed in Ref. 3. With increasing sideslip, Fig. 10 shows that vortex breakdown occurs above the wing at progressively lower angles of attack and there is evidence of this in Fig. 9, where there are marked kinks in the C_l plot at $\beta = +3°$ for $\alpha = 20°$. At $\alpha = 25°$, static measurements indicate a considerable reduction in l_v but the dynamic measurements show no such change. A reduction in l_v between $\alpha = 20°$ and 25° was also suggested in previous static tests[4] where the C_l *vs.* β slope was measured over a range of $\pm 2°$ sideslip. This difference between 'static' and 'dynamic' l_v shows that in certain flow conditions care must be taken in interpreting static measurements if the data are to be used in aircraft response calculations or simulation.

3.3.2. *Angular velocity derivatives.* As in rotary pitching tests where m_q and $m_{\dot{\alpha}}$ can only be measured in combination, i.e. $(m_q + m_{\dot{\alpha}})$, so in these lateral tests the rotary derivatives are measured in combination with the rate of change of sideslip derivatives in the form given in Section 3.1. The $\dot{v}$ derivatives were not measured separately in the present tests but Ref. 2 shows that for a HP 115 model they were small compared with the rotary derivatives except in the case of $y_{\dot{v}}$ compared with y_r. It was found that $y_{\dot{v}}$ could be as much as $-0{\cdot}1$ for the HP 115 and it may be assumed that a similar value applies to the BAC 221.

The combined derivatives $(n_r - n_{\dot{v}} \cos\alpha)$, $(y_r - y_{\dot{v}} \cos\alpha)$ and $(l_r - l_{\dot{v}} \cos\alpha)$ are plotted in Figs. 12 and 13. Overall scatter in the measurements is reasonably small and there are marked discontinuities in $(l_r - l_{\dot{v}} \cos\alpha)$. The reason for these discontinuities is unexplained; they occur at incidences above and below that at which vortex breakdown has been observed. But when the derivatives are compared in

*Unless otherwise stated, comments refer to magnitudes of derivatives.

Section 4 it will be seen that $(l_r - l_{\dot{v}} \cos \alpha)$ for the Concorde shows similar characteristics.

The roll derivatives $(n_p - n_{\dot{v}} \sin \alpha)$, $(y_p - y_{\dot{v}} \sin \alpha)$ and $(l_p + l_{\dot{v}} \sin \alpha)$ are plotted in Figs. 14, 15 and 16. The latter two derivatives are well-defined and show no significant changes between zero and $\pm 5°$ sideslip. $(n_p - n_{\dot{v}} \sin \alpha)$, as measured, is very small and the apparent difference between characteristics with and without sideslip is probably not significant. From the evidence in Ref. 2 the possible effects of frequency parameter must be considered, particularly in the case of $(n_p + n_{\dot{v}} \sin \alpha)$ and $(y_p + y_{\dot{v}} \sin \alpha)$. The roll mode frequency parameter was approximately 1·0 compared with the flight Dutch-roll frequency parameter between 0·08 and 0·17. In the HP 115 tests[2], an equivalent decrease showed a 25 per cent increase in the magnitudes of the yawing moment and side force derivatives at high angles of attack and the possibility of substantial differences between the tunnel-measured and flight values of these BAC 221 derivatives cannot be excluded. On the other hand, the HP 115 tests indicated that $(l_p + l_{\dot{v}} \sin \alpha)$ was not subject to a large frequency parameter effect and there can be more confidence in the accuracy of this derivative.

4. *Comparison of BAC 221, Concorde and HP 115 Results.*

The non-dimensional aerodynamic derivatives of these three aircraft are more easily compared if the reference area and length are similarly defined in each case. The reference area is defined as the gross wing plan area and in the case of the BAC 221 and the Concorde this includes the fuselage nose area as shown in Fig. 17 (Concorde wing area is not normally defined in this way). Wing span is used as the reference length. The wing planforms and the fuselage elevations are compared in Figs. 17 and 18 where the respective CGs have been aligned on a common reference axis. Sting axes shown are also the angle of attack datums and it should be noted that the HP 115 datum is 1·5° nose down relative to the wing centreline chord. Details of the three models and tests are given in Table 1.

The derivatives are compared in Figs. 19, 20 and 21. The rolling moment derivatives l_v, $(l_r - l_{\dot{v}} \cos \alpha)$ and $(l_p + l_{\dot{v}} \sin \alpha)$ are basically similar, as might be expected, since they are closely identified with the wing planforms which are all slender configurations of similar leading edge sweep angles. $(n_r - n_{\dot{v}} \cos \alpha)$ and y_v are also very similar but this may be fortuitous since the shape and area of the fuselage profiles would be expected to have significant effects on these derivatives and as Fig. 18 shows the elevations are not particularly similar. The characteristics of n_v for the HP 115 are quite different from those for the other two aircraft in that stability increases with angle of attack, as shown in Fig. 19. There is also a substantial and more or less constant difference between BAC 221 and Concorde n_v.

Substantial differences are apparent in the cross derivatives $(y_r - y_{\dot{v}} \cos \alpha)$, $(n_p + n_{\dot{v}} \sin \alpha)$ and $(y_p + y_{\dot{v}} \sin \alpha)$. No experimental points are shown for the latter two in the case of the HP 115 since these were obtained from a plot against frequency parameter at several angles of attack[2]. The comparison of these derivatives is complicated, not only because of their obscure origin but also because, for the sideforce and yawing moment derivatives at least, frequency parameter has a strong effect. The BAC 221 roll frequency parameter in the present measurements is substantially higher than that of any flight rigid body modes but flight and tunnel values of v are comparable both in the case of Concorde and HP 115.

The HP 115 tests of Ref. 2 showed that $(n_p + n_{\dot{v}} \sin \alpha)$ becomes more positive with increasing frequency parameter but it cannot be assumed that the relatively more positive $(n_p + n_{\dot{v}} \sin \alpha)$ for the BAC 221 is necessarily due to measurement at a high frequency parameter since Fig. 21 shows that for Concorde, even at $v = 0{\cdot}32$ this derivative is similar to that of the BAC 221.

Because of the marked scatter and variation with incidence of $(y_r - y_{\dot{v}} \cos \alpha)$ for Concorde, the experimental data was reanalysed but no reason could be found for rejecting the results, at least, as far as the general trend is concerned. It should also be noted that, from the evidence of Ref. 2, $(y_r - y_{\dot{v}} \cos \alpha)$ contains a substantial contribution from the $(y_{\dot{v}} \cos \alpha)$ term.

5. *Conclusions.*

A complete set of lateral aerodynamic derivatives has been measured on a 1/12 scale model of the BAC 221 from $\alpha = 0°$ to $\alpha = 26°$. The effects of sideslip were measured at four angles of attack. The results are considered to be generally reliable; there is good agreement between the static and dynamic measurements of the derivatives n_v, y_v and l_v, but at high angles of attack, in the presence of complicated

flow characteristics, determination of l_v from static tests is of doubtful validity.

Owing to certain features of the model it was not possible to obtain check measurements of n_v, y_v and l_v from the sideslipping mode.

A comparison of lateral derivatives of the BAC 221, Concorde and HP 115 shows that the rolling moment derivatives are similar but n_v and $(n_p + n_{\dot{v}} \sin \alpha)$ in particular, increase markedly with angle of attack for the HP 115 but not for the Concorde and BAC 221.

LIST OF SYMBOLS

b	Wing span
C_l	$\dfrac{L}{\frac{1}{2}\rho V^2 S}$, rolling-moment coefficient
C_n	$\dfrac{N}{\frac{1}{2}\rho V^2 S}$, yawing-moment coefficient
C_y	$\dfrac{Y}{\frac{1}{2}\rho V^2 S}$, sideforce coefficient
C_z	$\dfrac{Z}{\frac{1}{2}\rho V^2 S}$, normal-force coefficient
c_o	Reference chord
L	Rolling moment
l (with suffix)	Non-dimensional rolling-moment derivative
N	Yawing moment
n (with suffix)	Non-dimensional yawing-moment derivative
P	Angular velocity in roll
r	Angular velocity in yaw
S	Wing area
u, v, w	Body axes components of velocity
V	Free-stream velocity
Y	Sideforce
y	Sideways displacement
y (with suffix)	Non-dimensional sideforce derivative
α	Angle of incidence (relative to sting axis) } *see* footnote to para. 3.3.
β	Angle of sideslip }
ν	Frequency parameter
ρ	Air density

ϕ Angular displacement in roll

ψ Angular displacement in yaw

ω Circular frequency

Suffixes.

p, r, v, y, ϕ, ψ — Denote derivatives with respect to these variables

---

REFERENCES

No.	*Author(s)*	*Title, etc.*
1	J. S. Thompson and R. A. Fail	Oscillatory derivative measurements on sting-mounted wind-tunnel models at R.A.E. Bedford. R.A.E. Technical Report 66197 (AGARD C.P. 17) 1966.
2	J. S. Thompson, R. A. Fail and J. V. Inglesby ..	Low-speed wind-tunnel measurements of the oscillatory lateral stability derivatives for a model of a slender aircraft (HP 115) including the effects of frequency parameter. A.R.C. C.P. 1097. 1969.
3	R. F. A. Keating	R.A.E. Technical Report (to be published).
4	P. M. Murdin	Low-speed wind-tunnel tests on a 1/7 scale model of the BAC 221. R.A.E. Technical Report 69052. 1969.

TABLE 1

Model and Test Details.

	BAC 221	Concorde	HP 115
Model scale	1/12	1/30	1/8
Configuration	Clean, trimmed	U/C down, nose droop 17° Elevator set at 0°	U/C down Elevator set at 0°
Wing span, b	0·636 m	0·852 m	0·762 m
Wing area, S*	0·316 m^2	0·491 m^2	0·628 m^2
CG	0·362 m ahead of intersection of wing trailing edge and fuselage (flight CG)	0·525 c_o	0·548 c_o
Axes	body	body	body
Tunnel	13ft × 9ft	13ft × 9ft	13ft × 9ft and 8ft × 8ft
Tunnel speed, V	61 m/s	61 m/s	42·6 m/s, yaw and sideslip modes 91·5 m/s, roll mode
Reynolds number	2·66 × 10^6	3·55 × 10^6	2·35 × 10^6 and 2·15 × 10^6
Frequency parameter ν — yawing	0·30	0·20	0·18
Frequency parameter ν — sideslipping	0·52	0·42	0·31
Frequency parameter ν — rolling	1·00	0·32	0·55
Frequency parameter ν — flight dutch roll	0·08 to 0·17	0·38 at $\alpha \doteqdot 13°$	0·1 to 0·5

*To give a representative comparison of derivatives the Concorde wing area is as shown in Fig. 18. 'Standard' 1/30 scale Concorde S = 0·398 m^2.

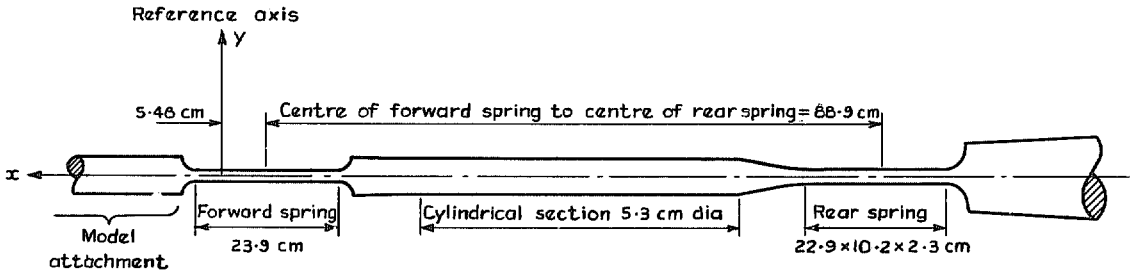

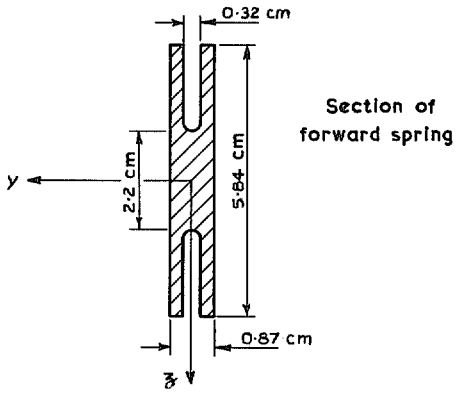

FIG. 1. Principal dimensions of spring unit.

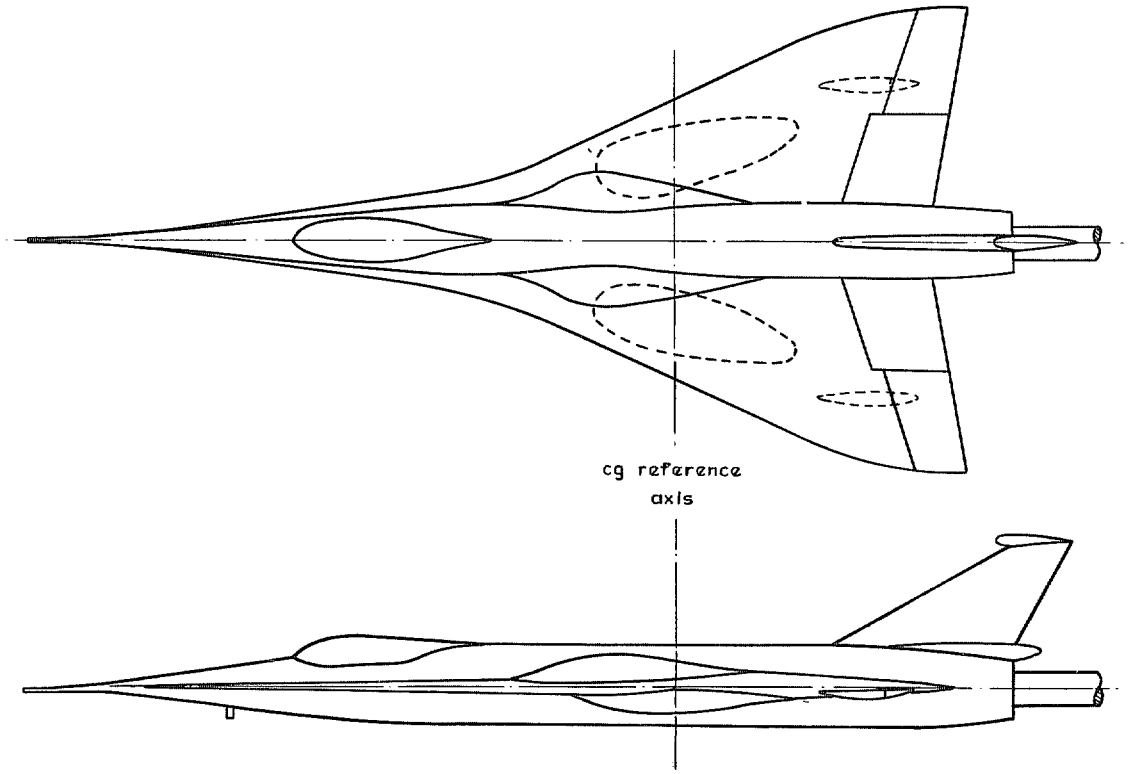

FIG. 2. Sketch of BAC 221 model.

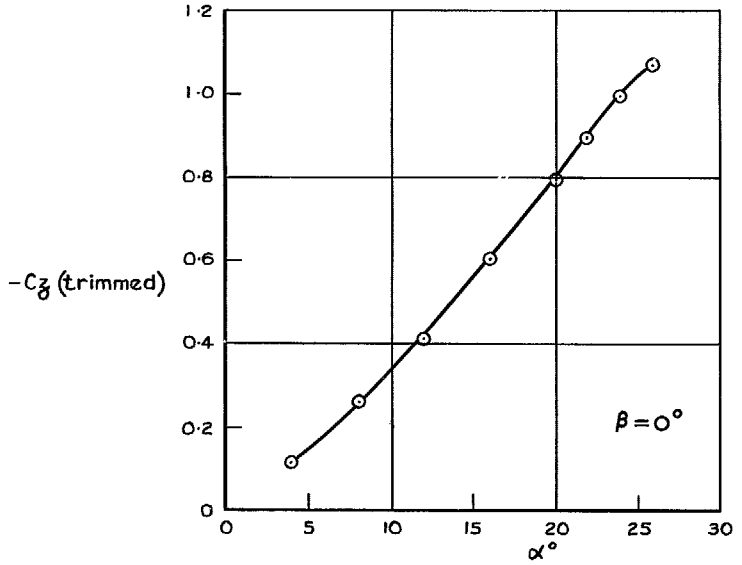

(a) $-C_z$(trimmed) v α°

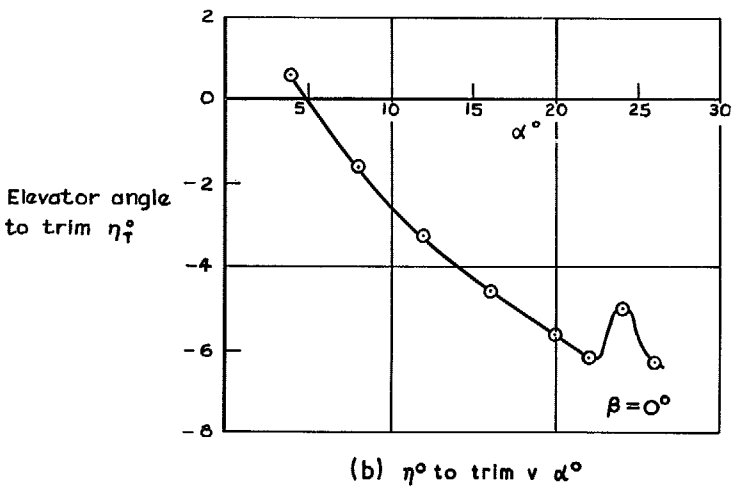

(b) η° to trim v α°

FIG. 3a & b. BAC 221 longitudinal trim characteristics.

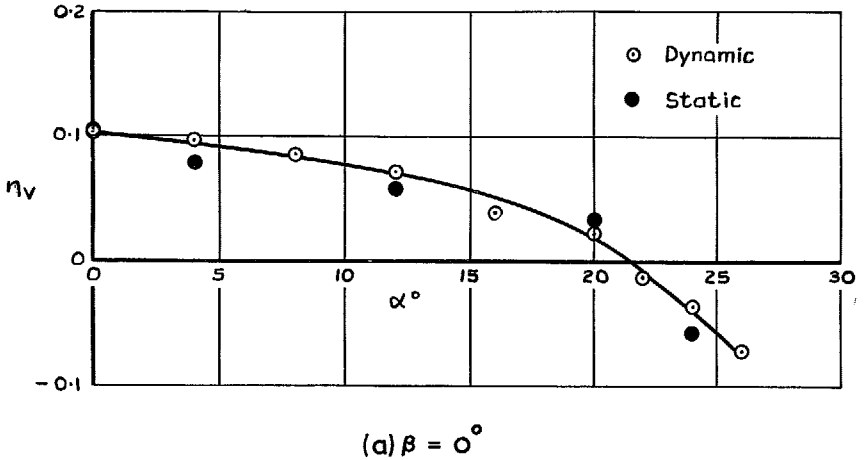

(a) β = 0°

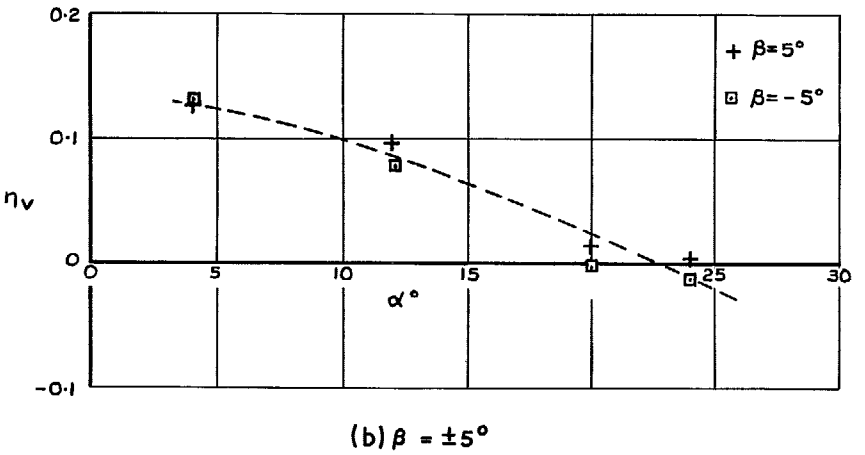

(b) β = ±5°

FIG. 4a & b. BAC 221 n_v *vs* α.

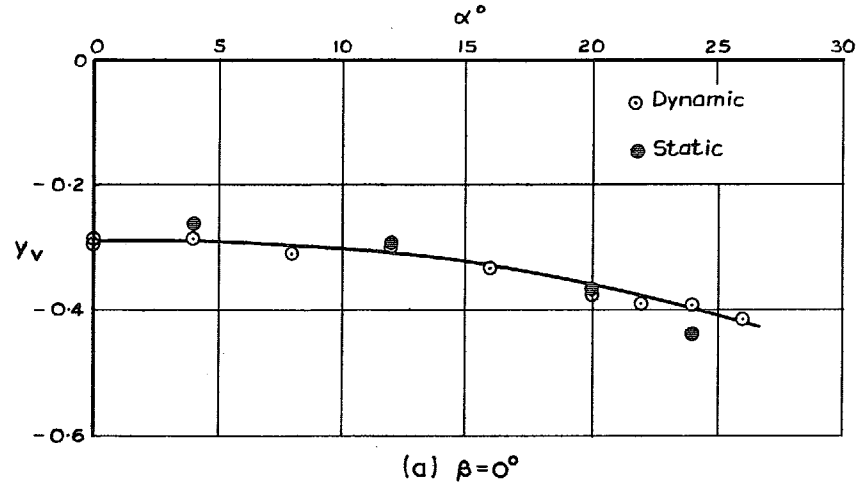

(a) β=0°

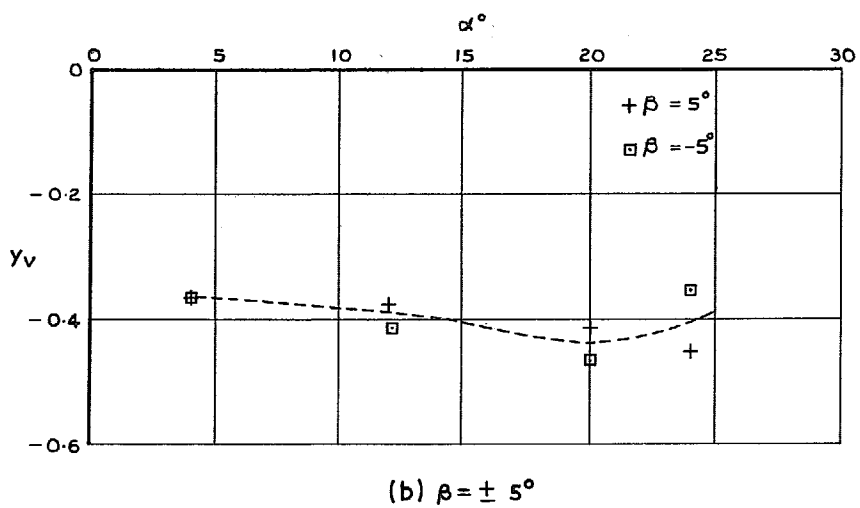

(b) β = ± 5°

FIG. 5a & b. BAC 221 y_v *vs* α.

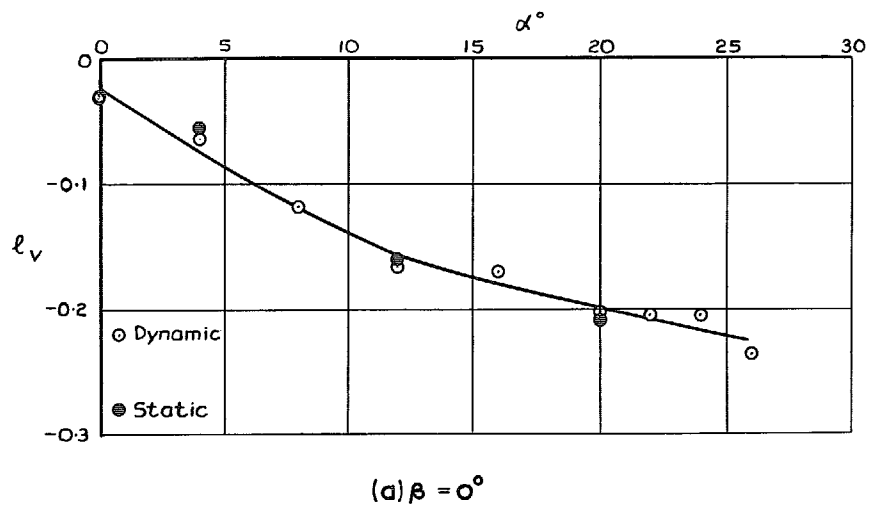

(a) β = 0°

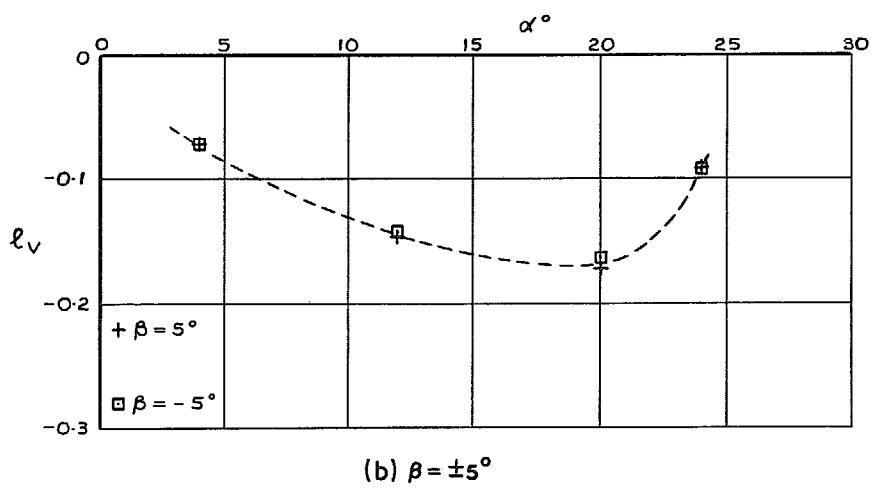

(b) β = ±5°

FIG. 6a & b. BAC 221 l_v *vs* α.

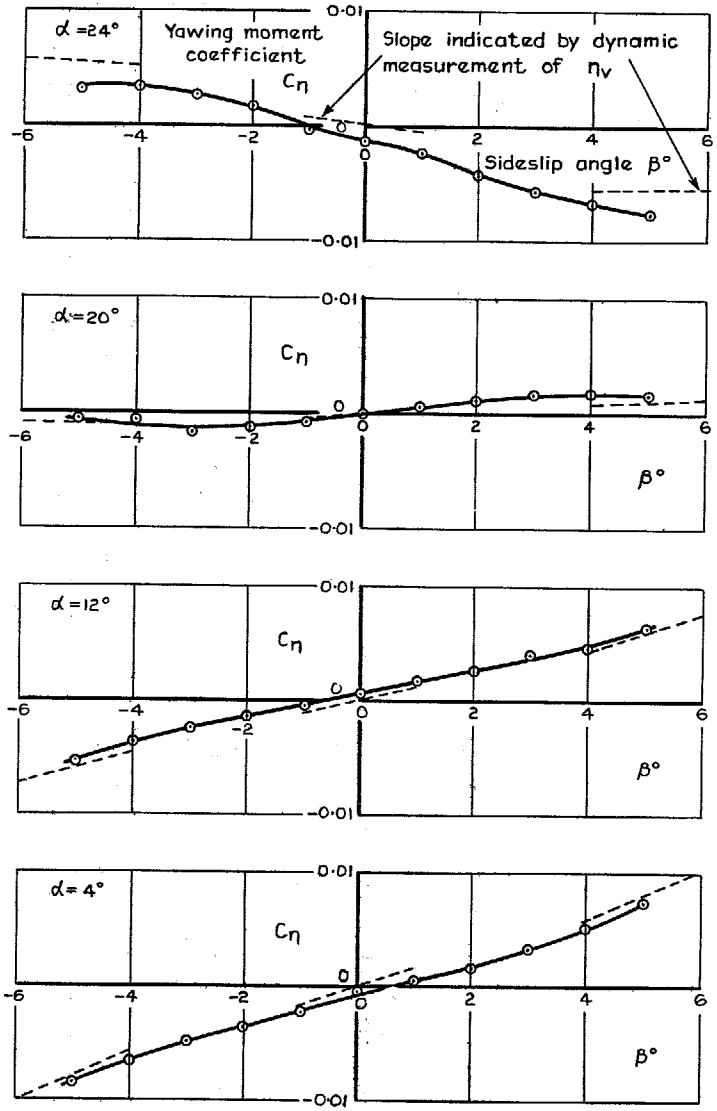

FIG. 7. BAC 221 C_n *vs* β.

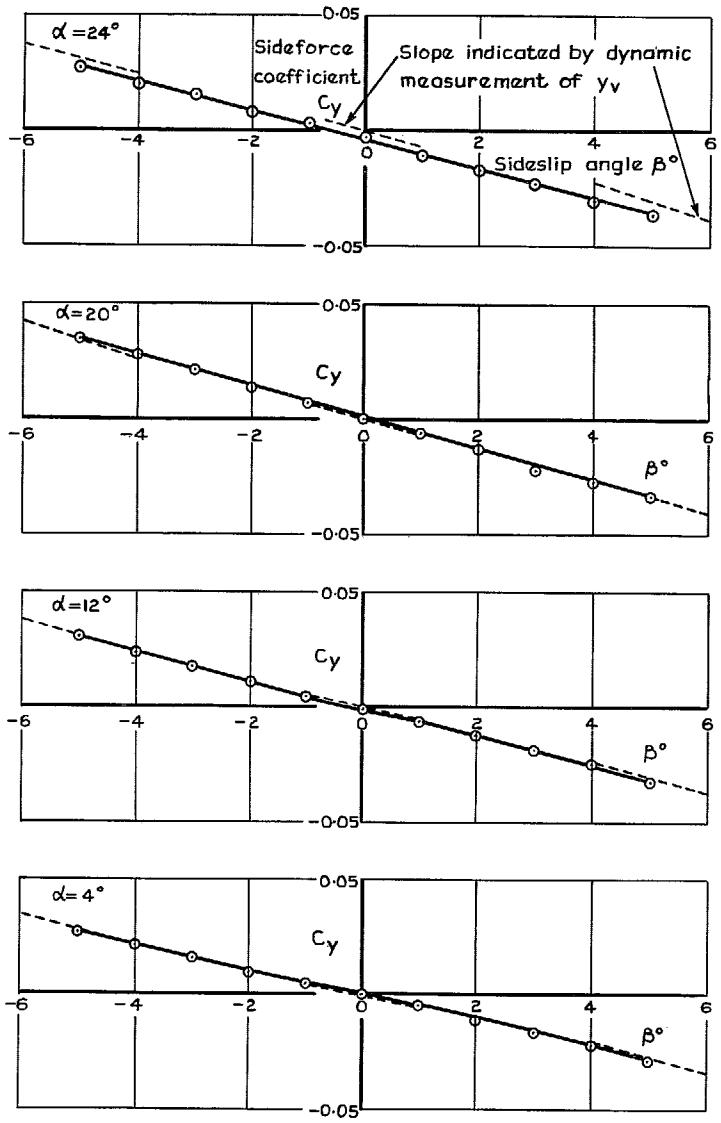

FIG. 8. BAC 221 C_y *vs* β.

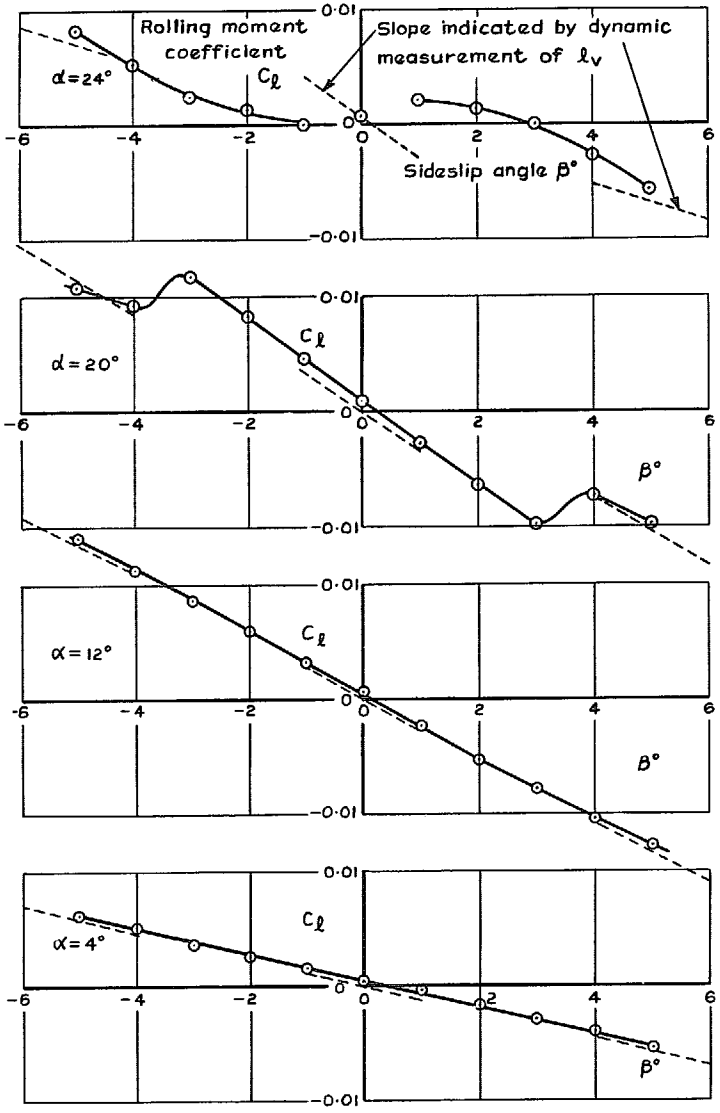

FIG. 9. BAC 221 C_l *vs* β.

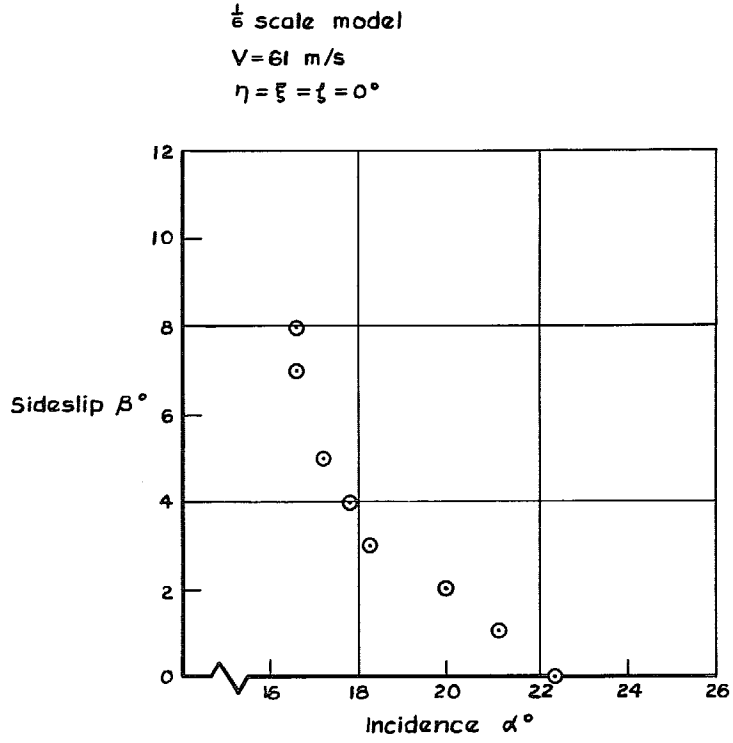

FIG. 10. Occurrence of vortex breakdown on the BAC 221. From tuft studies by Keating.

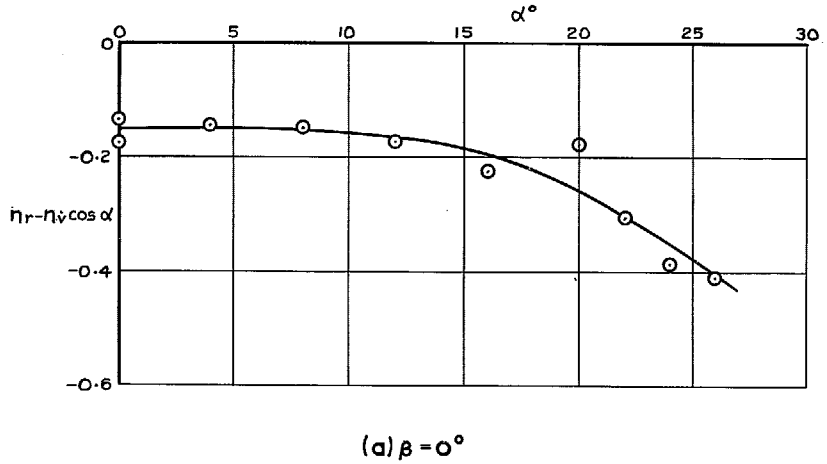

(a) $\beta = 0°$

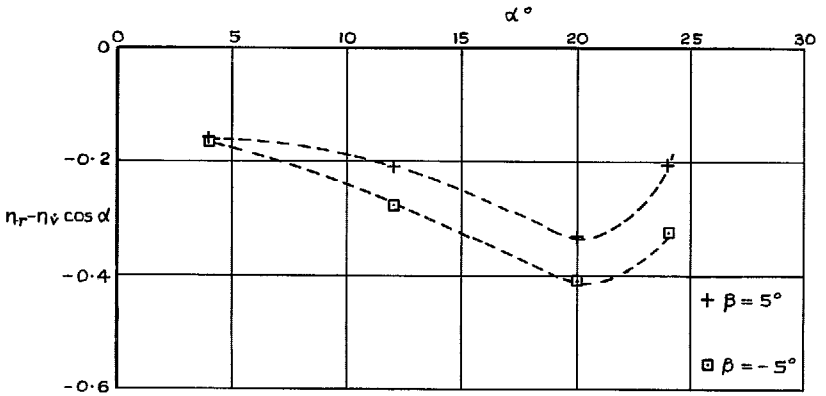

(b) $\beta = \pm 5°$

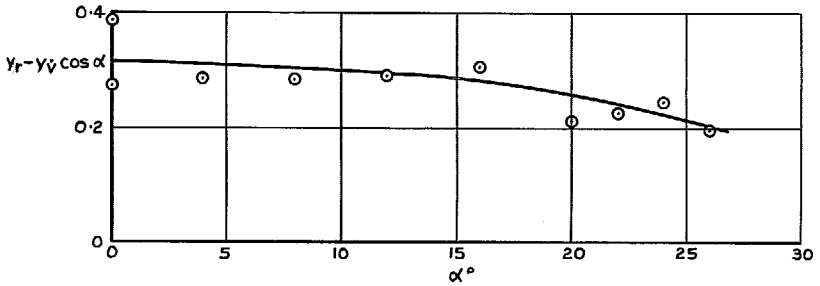

(a) $\beta = 0°$

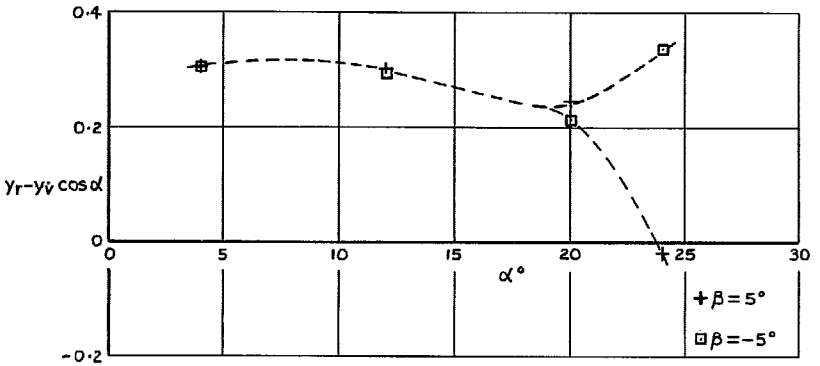

(b) $\beta = \pm 5°$

FIG. 11a & b. BAC 221 ($n_v - n_{\dot{v}} \cos\alpha$) *vs* α.

FIG. 12a & b. BAC 221 ($y_r - y_{\dot{v}} \cos\alpha$) *vs* α.

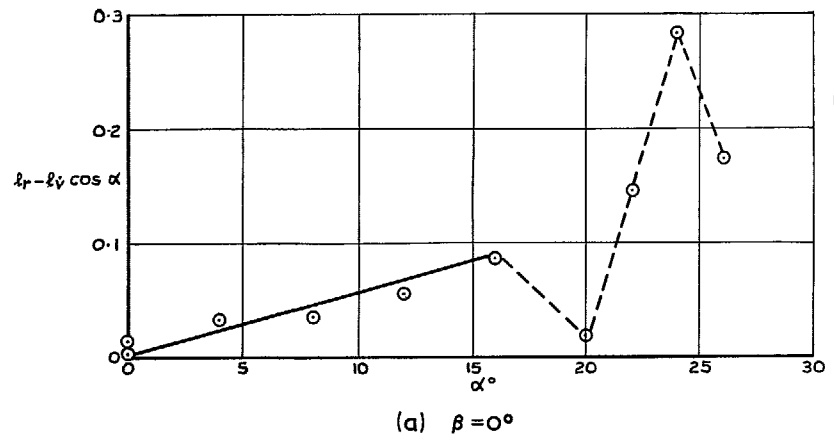

(a) $\beta = 0°$

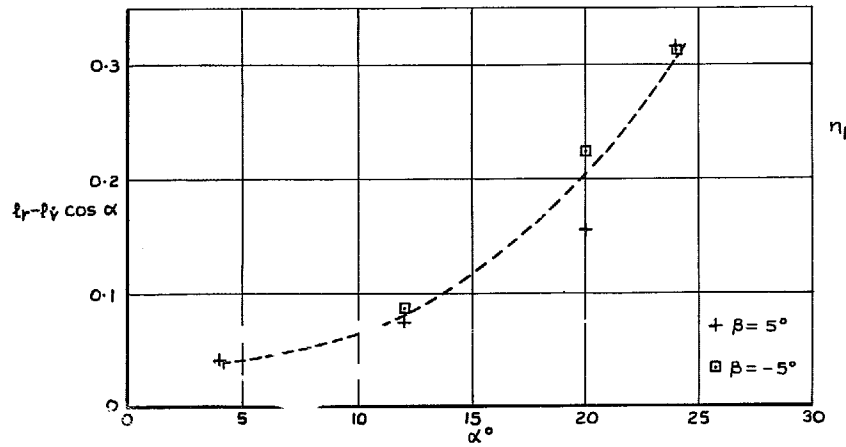

(b) $\beta = \pm 5°$

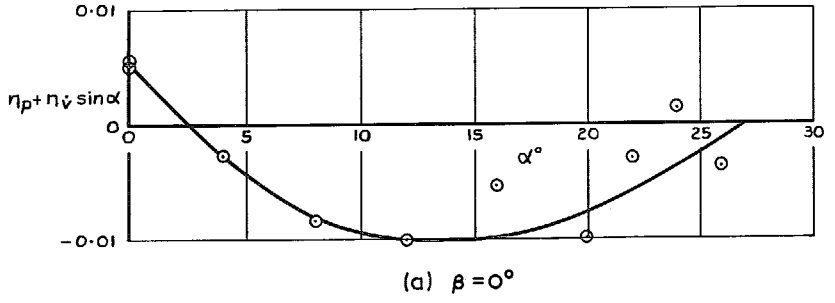

(a) $\beta = 0°$

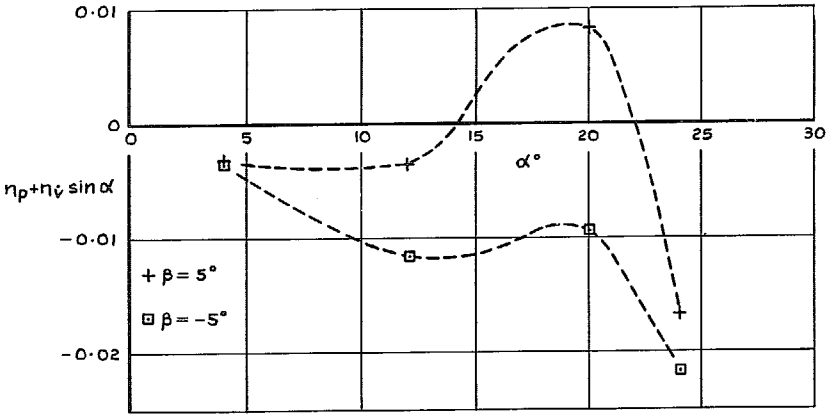

(b) $\beta = \pm 5°$

FIG. 13a & b. BAC 221 ($l_r - l_{\dot{v}} \cos \alpha$) *vs* α.

FIG. 14a & b. BAC 221 ($n_p + n_{\dot{v}} \sin \alpha$) *vs* α.

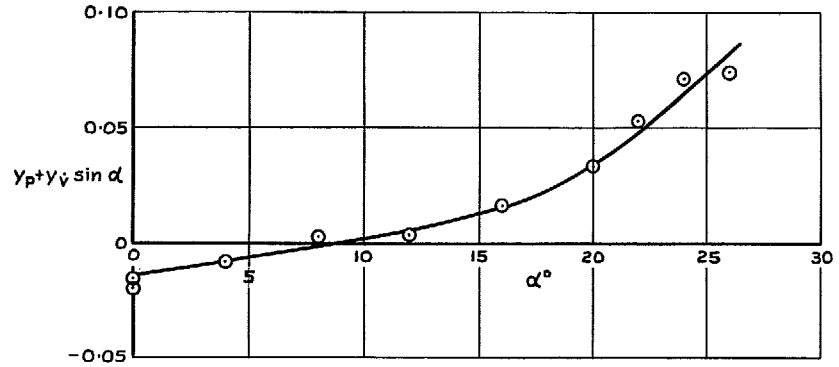

(a) $\beta = 0°$

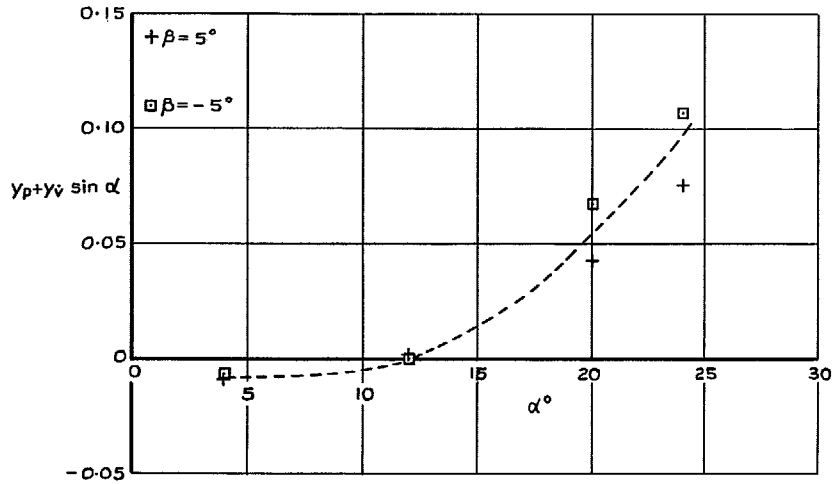

(b) $\beta = \pm 5°$

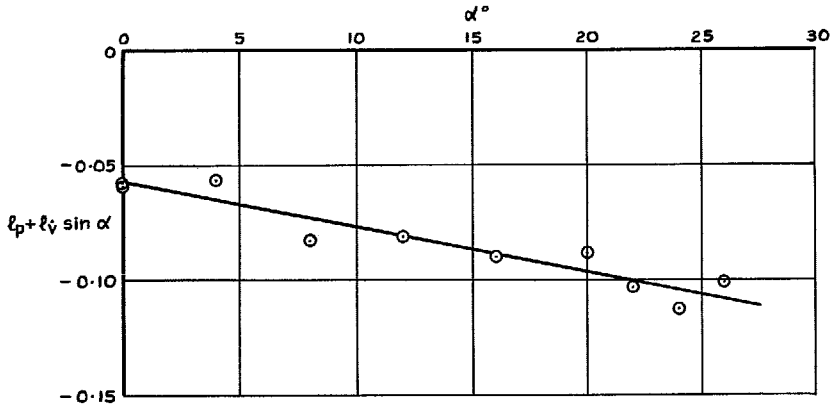

(a) $\beta = 0°$

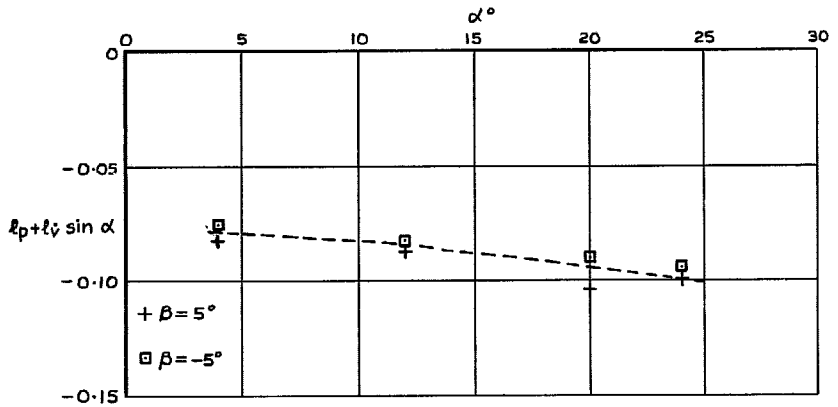

(b) $\beta = \pm 5°$

FIG. 15a & b. BAC 221 ($y_p + y_{\dot{v}} \sin \alpha$) *vs* α.

FIG. 16a & b. BAC 221 ($l_p + l_{\dot{v}} \sin \alpha$) *vs* α.

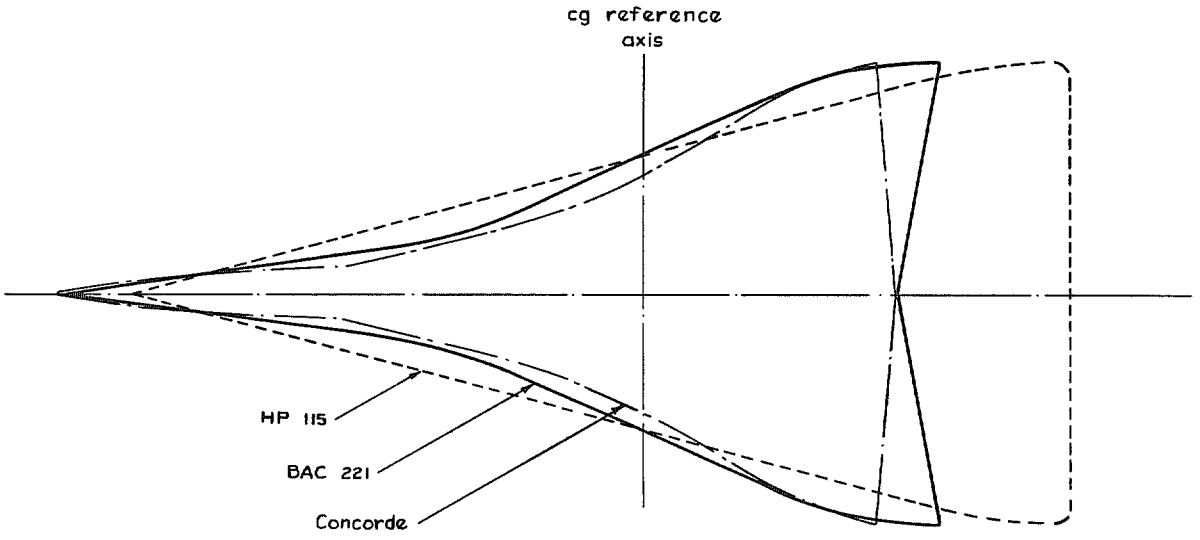

FIG. 17. Comparison of wing reference areas scaled to have equal spans.

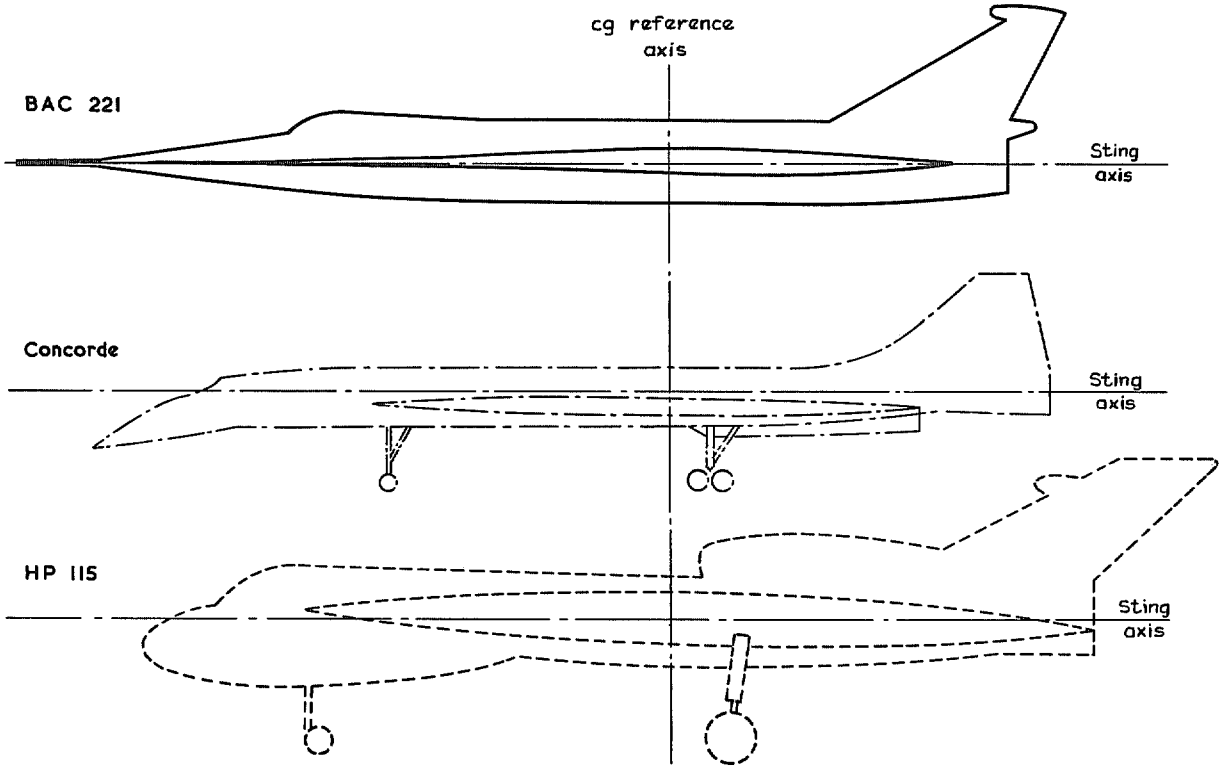

FIG. 18. Comparison of aircraft elevations scaled to have equal wing spans.

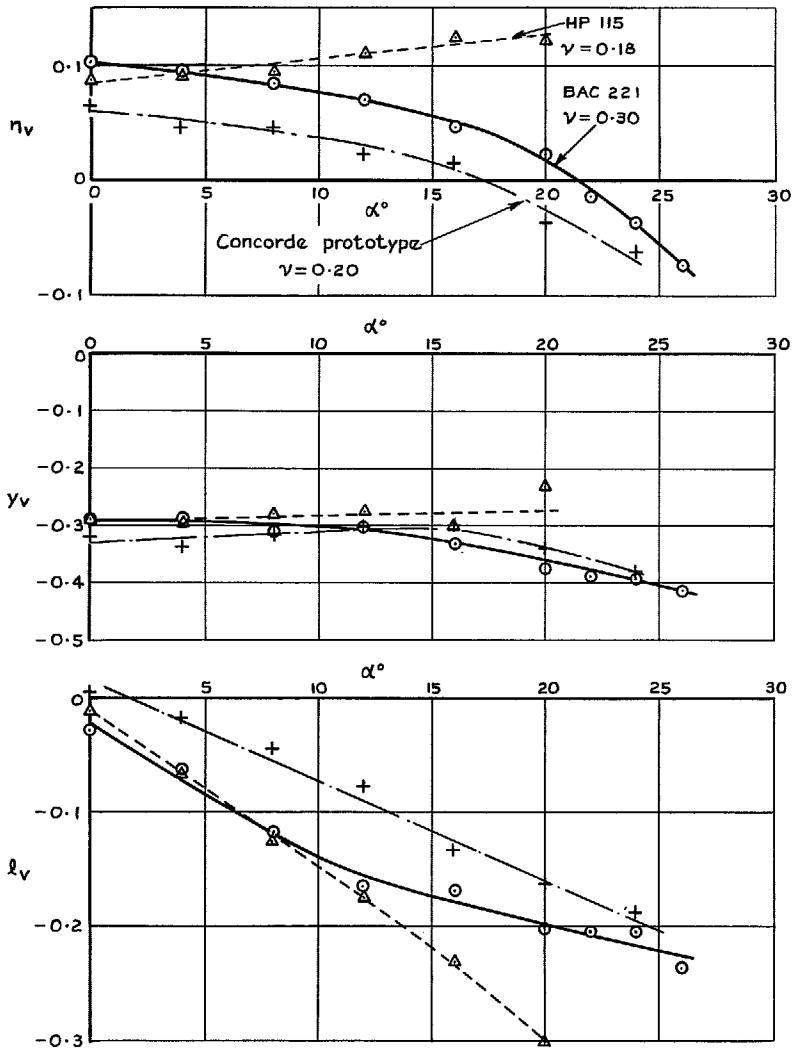

FIG. 19. Comparison of derivatives n_v, y_v and l_v.

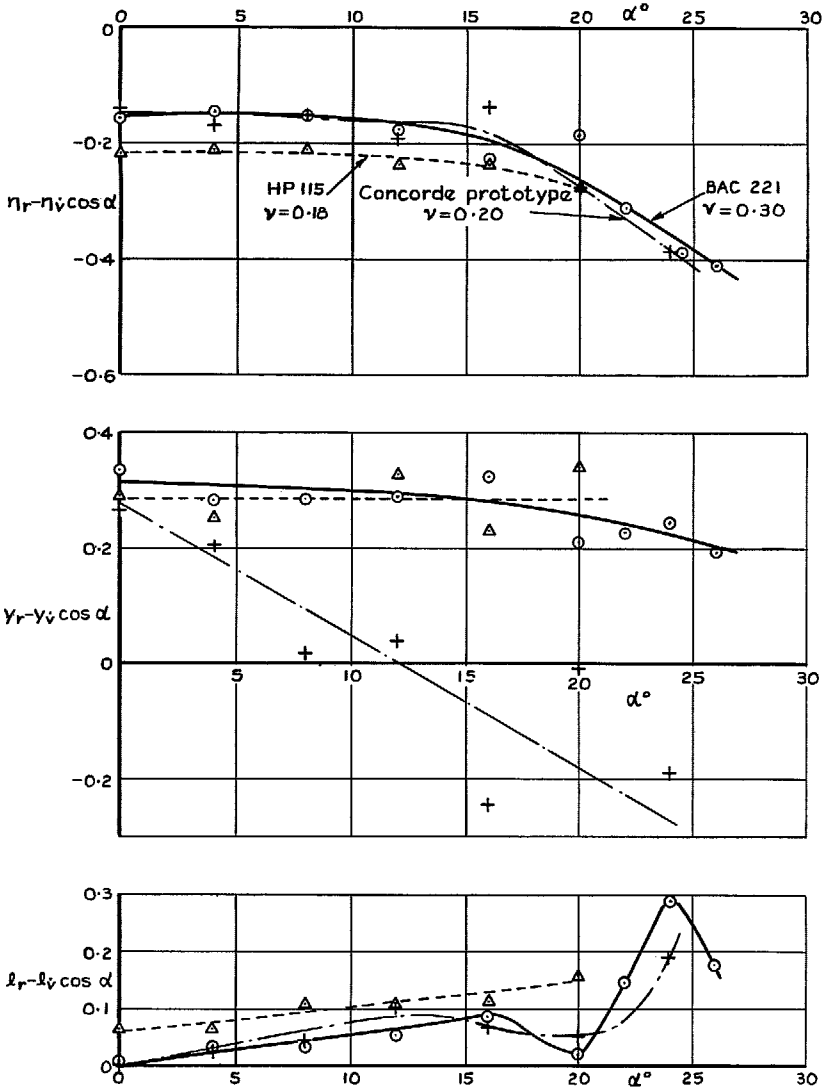

FIG. 20. Comparison of derivatives $(\eta_r + \eta_{\dot{v}} \cos\alpha)$, $(y_r + y_{\dot{v}} \cos\alpha)$ and $(l_r + l_{\dot{v}} \cos\alpha)$.

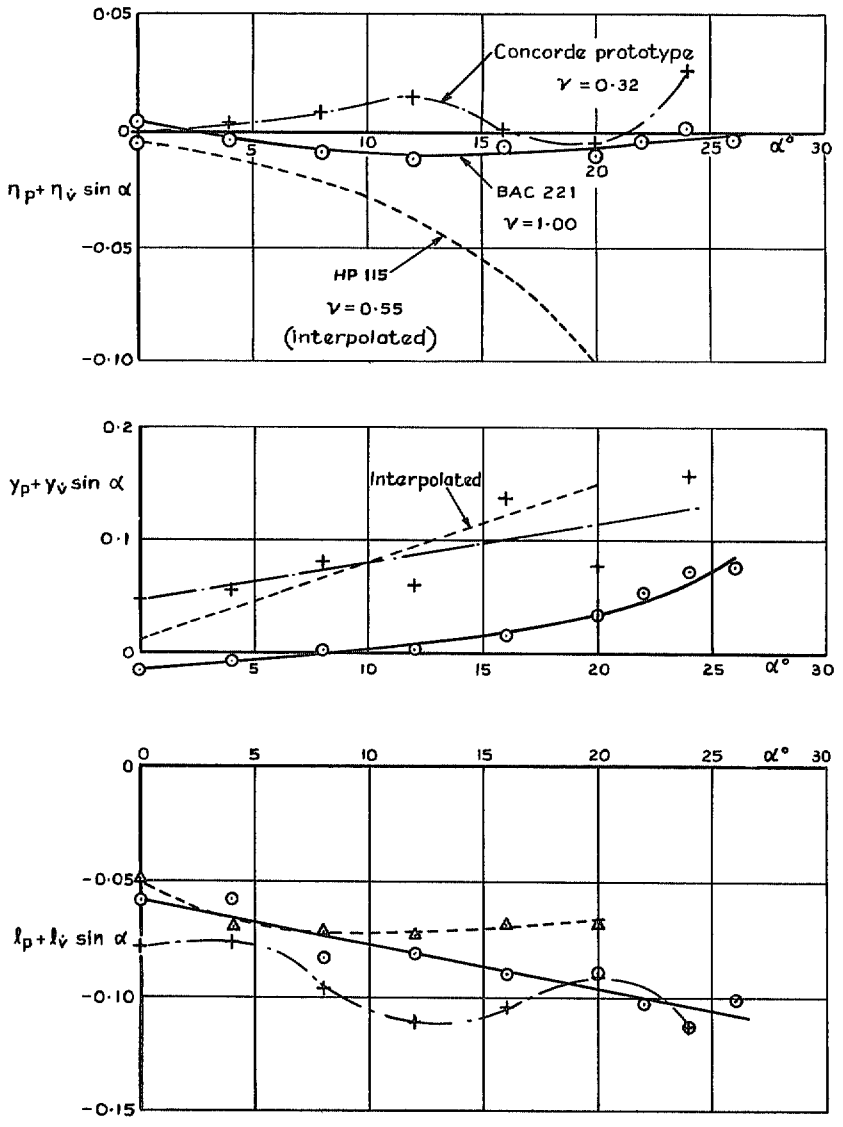

FIG. 21. Comparison of derivatives $(n_p + n_{\dot{v}} \sin \alpha)$, $(y_p + y_{\dot{v}} \sin \alpha)$ and $(l_p + l_{\dot{v}} \sin \alpha)$.

Printed in Wales for Her Majesty's Stationery Office by Allens Printers (Wales) Ltd.

Dd. 501372 K.5.

Published by
HER MAJESTY'S STATIONERY OFFICE

To be purchased from
49 High Holborn, London WC1V 6HB
13a Castle Street, Edinburgh EH2 3AR
109 St Mary Street, Cardiff CF1 1JW
Brazennose Street, Manchester M60 8AS
50 Fairfax Street, Bristol BS1 3DE
258 Broad Street, Birmingham B1 2HE
80 Chichester Street, Belfast BT1 4JY
or through booksellers

R. & M. No. 3671

SBN 11 470411 2